International Journal of Fatigue 143 (2021) 106011

Contents lists available at ScienceDirect

International Journal of Fatigue

journal homepage: www.elsevier.com/locate/ijfatigue

Experimental and numerical fretting fatigue using a new test fixture

Steffen L. Sunde *, Bjørn Haugen, Filippo Berto

Norwegian University of Science and Technology, Dept. of Mech. and Industrial Engineering, Trondheim, Norway

ARTICLE INFO

Keywords:
Fretting fatigue
Critical plane
TCD
Ruiz
Ti-6Al-4V

ABSTRACT

A unique dovetail-based test fixture for fretting fatigue was designed and is demonstrated with a combined experimental and numerical campaign. Fretting fatigue damage is analysed and correlated with numerical analyses using a modern Ruiz formulation and Findley critical plane parameter with the Theory of Critical Distances. Initial test results show that a simple critical plane model correlates life and cracking directions with experiments; however, the Ruiz parameter only serves as a hot-spot indicator. The fixture is designed to permit testing in submerged conditions and to allow additional loads to the specimens by using a multi-axial fatigue machine.

1. Introduction

Fretting is a concern arising from metallic components in contact, subjected to oscillating forces. Highly localized contact stresses and small relative movements cause surface damage and if the bulk stresses are high enough, fretting cracks propagate and cause *fretting fatigue*.

The features of fretting fatigue are quite complex with numerous interconnected parameters [1,2]. Most importantly are the conditions of the contacting surfaces, material properties and multi-axial non-proportional stress variations with steep gradients. Although fretting and fretting fatigue has been studied for over a century, it is still not fully understood. The chaotic synthesis of all the involved mechanisms makes the assessment very difficult, both in terms of analysis and in terms of experimental testing.

When analysing and predicting fretting fatigue, engineers are often faced with large geometries subjected to complex loads. Complete fretting assessments are next to impossible, because it would require considering a large array of different mechanisms in combination. Hence, simple assumptions are made and only a few key mechanisms are included in the analysis to make the problem practical. With respect to physical testing of fretting, careful control and monitoring the different mechanisms are difficult, and to isolate contact features for the analysis is challenging.

A number of different fretting fatigue test configurations have been devised throughout the years, starting from quite simple fatigue machines with "bridge-type" contact pads [3] to general fretting machines with multiple actuators and load cells capable of varying the fatigue loads, contact pressure and sliding force independently [2]. The most "classical" geometry for fretting fatigue is, perhaps, the dovetail joint studied by Ruiz et al. [4] and followed by many others [5–8]. Fretting fatigue in the dovetail joints of aircraft turbine blades is an important application and has been the target for much research. This test configuration is also quite popular due to its simplicity; there is no need for a specialized multi-actuator fatigue machine. A simple pulling action is used to simulate the centripetal forces acting on the turbine blade during operations. Optionally, additional actuators or shakers can used to apply the vibrational excitations from structure, aerodynamics, etc. [9].

In this work, yet another test fixture based on the dovetail joint is presented. This is the starting initiative for a new test program being developed, aiming at numerical and experimental investigations of fretting fatigue conditions relevant for engineering. The fixture presented here has some interesting additions when compared to previously developed dovetail test fixtures, as will be described in the following section. The main aim of this paper is to demonstrate the use of this new fixture, prove its usefulness in studying fretting fatigue and to address its potential to study a wide range of contact conditions. A long-term goal is to provide with useful experimental data and, with its accompanying numerical analysis, to permit scaled-down tests to apply to engineering components.

2. Experimental testing

The main advantages of the dovetail joint as a test setup for fretting fatigue is that it is easy to arrange and does not require special fatigue machines. The *disadvantage* is that there is much less control of the

* Corresponding author.
E-mail address: steffen.sunde@ntnu.no (S.L. Sunde).

https://doi.org/10.1016/j.ijfatigue.2020.106011
Received 31 July 2020; Received in revised form 17 October 2020; Accepted 20 October 2020
Available online 7 November 2020

contact pressure and shear stress, compared to bi-axial fretting rigs [10,11]. Several additions are introduced to the fixture shown in this work, see Fig. 1. Due to high stiffness of the lower fixture flange, a wide range of loads and specimen sizes are permitted. As the tension on the specimens increases, so does the wedge opening effect on the gripping mechanism, increasing the contact angle and altering the contact tractions. The width of the lower flange provide a possible additional source of excitation when using a multiaxial fatigue machine; By having two specimens with a *radial offset*, as shown in Fig. 1, a small torque can be applied to the specimens. The added force come, however, at the cost of some contact edge-effects as the contact pressure will vary over the specimen width.

The contact pads are slid into carefully machined slots. This allows for easily interchangeable contact pads and consequently permits testing with different contact geometries, surface treatments, material combinations, etc.

The lower gripping flange front and back sides can be enclosed, enabling submerged contact conditions. The rig is small enough to fit inside the temperature chamber for testing in elevated temperatures which is relevant for turbine blade dovetail joints. If the lower gripping flange is not enclosed, contact slip conditions and specimen strain can be analysed using *Digital Image Correlation* (DIC) techniques as performed in previous studies, see e.g. [12–14].

One of the main difficulties with the dovetail configuration is determining the appropriate loading conditions. A numerical analysis for each test program is necessary to determine the contact conditions and slip regimes for the given loads and geometry. For sharp-edged contact pads, the specimen can experience local plasticity even though the bulk loads are too small for fretting cracks to propagate. A large unknown in all types of fretting tests is the coefficient of friction (COF), which determines the contact conditions. The COF value is a *system* parameter and depends on not only material combination but loading, roughness, hardness, environment, sliding distance, geometry, etc.

A set of specimens is made in Grade 5 Ti-6Al-4V titanium alloy (see Tables 1 and 2) which is a commonly used alloy for fretting fatigue studies. The combination of low density, high strength and excellent heat resistance and bio-compatibility makes the alloy useful for aviation applications and orthopedic implants, among other fretting-critical fields. The geometrical details of the dovetail specimen and the contact pad is shown in Fig. 2. Note that the contact pads in this particular study have rounded contact profile.

The chemical composition of specimens material prior to machining is given in Table 2.

The material is rolled and cut using EDM wire machine and the specimen sides were machined flat. Rolled titanium is highly anisotropic with elongated grains and EDM wire cutting produces a surface with melted particles, micro-cracks and altered hardness. In other words,

Table 1
Mechanical material parameters from material certificate in accordance with ASTM E8/E8M-15a.

Tensile str. MPa	Yield str. (0.2%) MPa	Hardness HV	Ra μm
920	838	301	⩽3.2

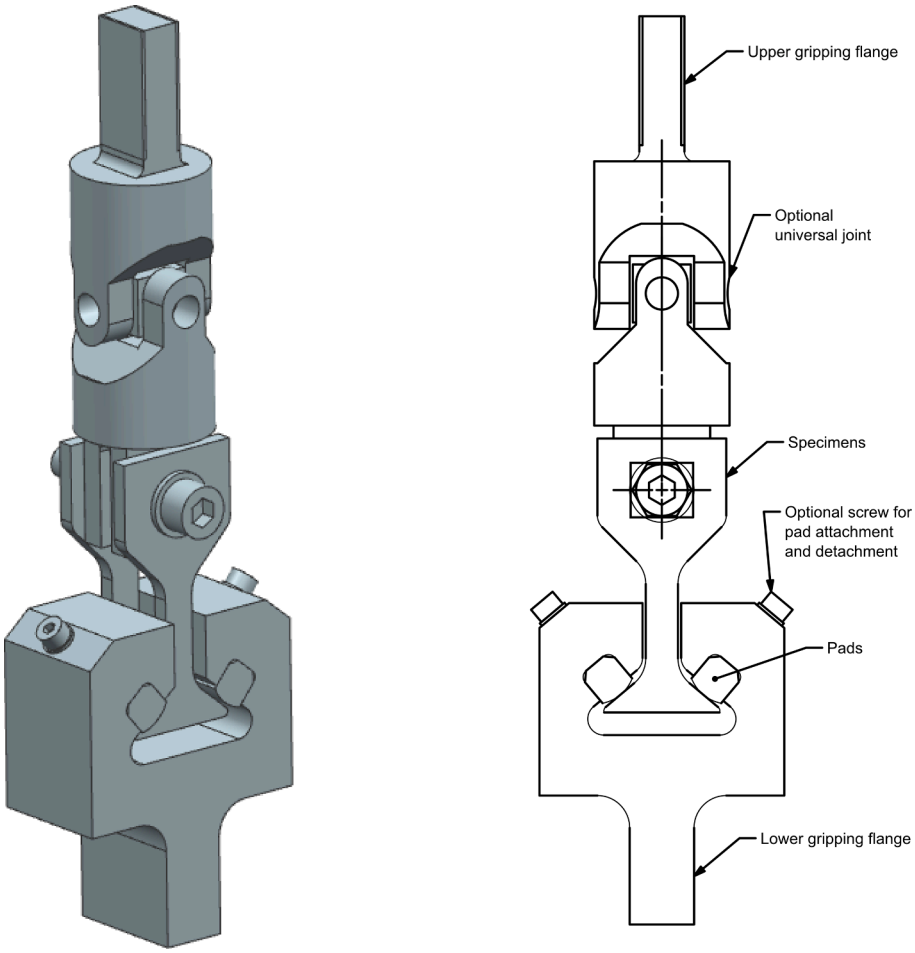

Fig. 1. Dovetail fixture arrangement. A universal joint is used to make the test rig self-align when the axial loads are applied, providing symmetric loads to the specimens.

Table 2
Chemical composition of specimens according in accordance with ASTM B348-13, forged annealed and peeled.

Al	Fe	C	N	O	H	V
6.23	0.03	0.01	<0.01	0.13	0.003	4.1

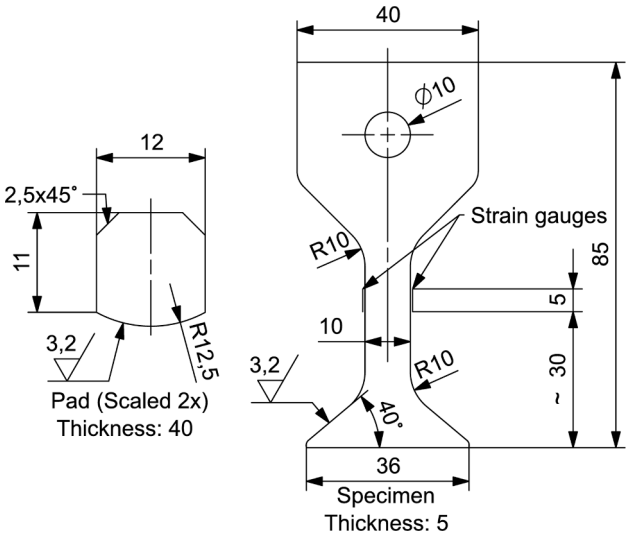

Fig. 2. Geometric details of the specimen and contact pad used in this paper. General tolerances are in accordance with ISO 2768-m. Units are in millimetres.

there are factors of uncertainty related to the material and specimen surfaces. For many engineering applications, EDM wire cutting is an appropriate manufacturing method due to its efficiency and precision. Consequently, fretting fatigue performance of such surfaces are of interest despite its inherent uncertainty.

Hardness of the contacting surfaces was tested using pyramid diamond indenter with 1 kg force for four seconds. The hardness of the EDM wired surfaces was found to be approx. 300 HV1 and the machined surfaces were around 350 HV1. Fig. 10 shows a Scanning Electron Microscope (SEM) picture of the surface where quite irregular surfaces can be seen with round, melted drops. The edges of the samples were deburred by grinding, causing potential crack initiation points and some uncertainties for the contact area. Specimens were cleaned using ethanol immediately before testing.

A *MTS 809 Axial/Torsional test system* fatigue machine was used to apply uniaxial fretting load to a single specimen at a time (see Fig. 3). A universal joint was used to avoid over-constrained specimens to be loaded asymmetrically. A Peak-Valley compensator in the test controller was used, allowing for testing at higher frequencies whilst maintaining full load ranges. Load and displacement were recorded during testing and a pre-determined stopping criterion was assigned to the displacement signal so that the test would stop when a crack had caused the sample to elongate. A subset of samples were also equipped with strain gauges on both flanks in order to more accurately record specimen behaviour during the test (see Fig. 2). Load and displacement data were logged at 50 Hz using the built-in load cell in the fatigue machine. FLAB-5-11 strain gauges (TOKYO Sokki Kenkyujo Co. Ltd.) were recorded using a HBM MX1615B amplifier at 300 Hz, resulting in large amounts of data.

3. Numerical modelling

A series of 2D finite element analyses (FEA) were performed to evaluate the design and to compare numerical predictions of fretting fatigue performance with experimental results. FEA is often the

Fig. 3. Fixture mounted in multiaxial fatigue machine with a single Ti-6Al-4V specimen instrumented with strain gauges on both flanks.

preferred method of solving fretting fatigue contact, providing accurate contact stresses and strains. For the case of uni-axially loaded specimen, symmetry conditions permit the FE model to be halved, see Fig. 4. Reference points are used as control nodes in top and bottom of the model and kinematic couplings are used to attach the model degrees of freedom to boundary conditions and loads. Abaqus 2017 FE software

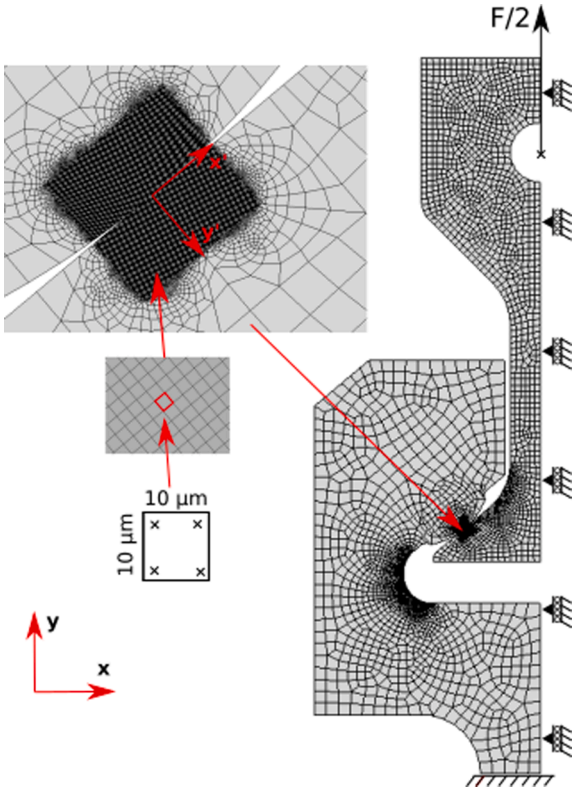

Fig. 4. 2D Finite element model. Symmetry conditions ($u_x = r_y = r_z = 0$) is applied along the centreline and bottom are fixed ($u_y = 0$). Contact and sub-surface area are meshed with structured bi-linear elements.

package was used to solve for the stresses and strains. Python was used to extract results and parallelised C++ was used to perform critical plane computations.

Four-noded (bi-linear) plane strain elements were used due to spatially small stress gradient compared to specimen width. Approximate global element size for the fixture is 2 mm and refined in critical areas according to a thorough stress convergence study. Element size in the chamber fillet is approximately 0.125 mm. For the specimens 1 mm elements were used globally and refined to 0.25 mm at the fillet. Mesh was allowed to be unstructured for the majority of the model, but structured mesh is used for the subsurface material (see Fig. 4). For accurate contact slip and stresses, a very fine mesh of 10 μm was required in areas surrounding the contact. Due to the severe stress gradients and micro-sliding, a highly refined mesh is necessary. It is not uncommon with element sizes in fretting studies to be in the ranges of 10–50 μm and even down to 2–5 μm [15]. Here, contact stresses converge rather quickly but for accurate values of relative movement (slip) a fine mesh is important. A high resolution of subsurface stresses is also useful for the critical plane post-processing stage when averaging techniques are used, see Section 3.3. Material elasticity parameters for Ti-6Al-4V used here are as were Young's modulus of 115 GPa and Poisson's ratio of 0.32 [1].

Contact analyses are performed using Coloumb friction with two different values for COF. To ensure accurate contact solutions, the fretting interface is modelled using Lagrangian multipliers for normal and tangential behaviour. Lagrangian multipliers introduces extra degrees of freedom to accurately solve the frictional sliding between the master and slave body, pad and specimen respectively. Whilst a "penalty" formulation is much simpler numerically, and sufficiently accurate for contact stress analysis in many cases, the Lagrangian multipliers are used if the contact slip conditions are important. "Hard" normal conditions will cause FE solver iterations to enforce that no slave surface nodes penetrate master surface elements. In some cases hard contact makes convergence more difficult, but will provide more accurate results. A precise value for the COF is difficult to obtain, even through extensive testing. Here, COF is not measured explicitly but numerical simulations are performed with two different values, 0.55 borrowed from [1] and one higher value of 0.70 [16]. Although often simplified as being dependant only on the two materials in contact, COF is a systems property and is depending on numerous factors, e.g. contact pressure, surface roughness, environmental conditions, etc. Therefore, it is reasonable to think that the COF itself will change throughout the fretting life, particularly if frictional wear or plastic deformation alter the contact conditions. Friction is known to be especially difficult to represent in fretting fatigue, and is often reported to increase during fretting life [17,16,18].

As the stress state in the contact area is assumed to be in plane strain, the stress tensor is on the form

$$\boldsymbol{\sigma}(t) = \begin{bmatrix} \sigma_{xx}(t) & \sigma_{xy}(t) & 0 \\ \sigma_{xy}(t) & \sigma_{yy}(t) & 0 \\ 0 & 0 & \sigma_{zz}(t) \end{bmatrix} \tag{1}$$

That is, the stress is three-axial with an out-of-plane z-component owing to the material contraction due to the Poisson effect. It can be shown to be reduced to a 2D problem, but is here solved using a general three-dimensional post-processing code [19]. A separate, rotated coordinate system is placed in the center of contact, as shown in Fig. 8. The stresses are solved for at the element integration points and extrapolated to the element nodes. They are then averaged for each connected element to obtain the global nodal values. Subsequently, stresses are transformed to the local contact coordinate system and extracted for a subset of elements beneath the contact surface as shown in Fig. 4.

3.1. Contact analysis

Since contact normal load and tangential load for the dovetail in general vary proportionally, a Hertzian (cylinder on plane) type of contact forms and grows in magnitude as axial load is increased. When the load is released, shear instantly changes direction at the outer edges of contact where the local frictional resistance is low. Now a partial slip conditions appears, qualitatively comparable with the classical Cattaneo-Mindlin (CM) solution [20,21]. In the CM solution however, normal load is constant as the tangential load is gradually applied and kept within frictional load.

Initially, during ramp loading, contact is in gross slip conditions, as can be seen in Fig. 5. During the cyclic loading however, partial slip is seen with the boundary between stick and slip changes continuously. Therefore, a quite large area becomes severely fretted, causing multiple potential sites for crack initiation. The value of Q/P is usually lower than the average coefficient of friction, except during the ramping step.

The classical works by Ruiz et al. [4] presented two different mathematical parameters specific to fretting and fretting fatigue. The first parameter (here denoted k_1 to meet the original notation) was obtained by simply multiplying the largest tangential stress by the maximised frictional work, thus being expressed as

$$k_1 = (\sigma_{xx})_{max} \cdot (\tau\delta)_{max} \tag{2}$$

where σ_{xx} is the stress component acting parallel to the contact surface, τ is the shear stress and δ is the relative slip. Previous studies, such as [22,19] notes that this parameter is slightly inconvenient due to the maximum frictional work and maximum tangential stress potentially occurring at different locations. Thus obviously not being physically sound. Ruiz et al. [4] also noted that, although they found reasonable agreement with experiments performed for dovetail specimens, k_1 did not indicate *cracking location* particularly accurate. An alternative, empirical parameter was therefore proposed,

$$k_2 = \sigma_{xx} \cdot \tau\delta \tag{3}$$

Thus, fretting fatigue damage is quantified by the product of shear work ($\tau\delta$) and stress component acting parallel to the contact surface. Numerically, the parameter k_2 is evaluated by integrating the specific shear work over the fretting cycle, like in more recent versions of the Ruiz criterion [23–25]. A considerable advantage of this parameter over k_1 is that its local and can that it can easily be integrated over the fretted surface (see Fig. 6). However, it is clear that, the Ruiz' parameters lack in terms of physical interpretation [5,2]. Regarding k_2 and as material parameters is somewhat artificial, but nonetheless serves as a means of comparison and is widely used in engineering practice [26,27]. Also note that the parameters k_1 and k_2 are one-dimensional in this form but can be extended to use for 3D models [25,28].

3.2. Critical plane analysis

As indicated in the previous section, simple fretting parameters like Ruiz and its derivatives are very accessible and sometimes useful for qualitative comparisons of different fretting situations. These parameters can provide hot-spot indications but for more quantitative analyses like life predictions, more thorough analysis is required and physical criteria are preferred. Fretting fatigue crack nucleation in mixed and partial slip regimes is commonly evaluated by using multiaxial fatigue methods [29–33].

Here, stresses are extracted for eight time steps of the loading cycle, for a node set representing the specimen subsurface and stored in separate files. A critical plane post-processing procedure is then carried out using the Findley parameter [34] for a variety of conditions. Since the coefficient of friction is not known accurately for the actual system, the critical plane analysis is made for a set of different values of COF (see Fig. 14).

The multi-axial fatigue parameter proposed by Findley in the sixties combines the shear loads with the normal loads. More specifically, the critical plane is defined as the candidate material plane (π) experiencing

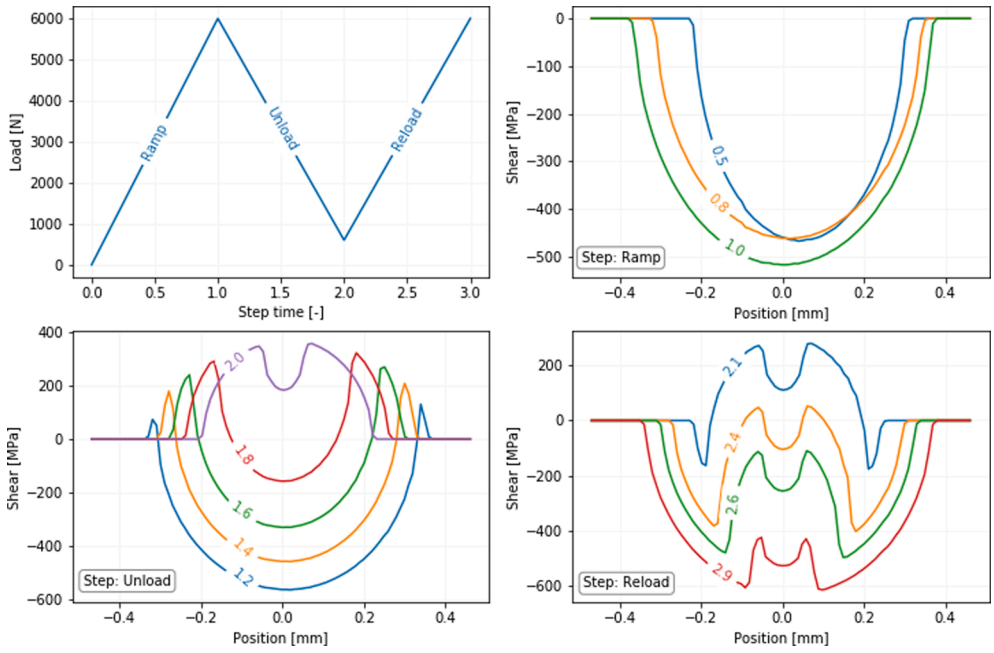

Fig. 5. Contact shear evolution for test case 6 (T6), see Table 3.

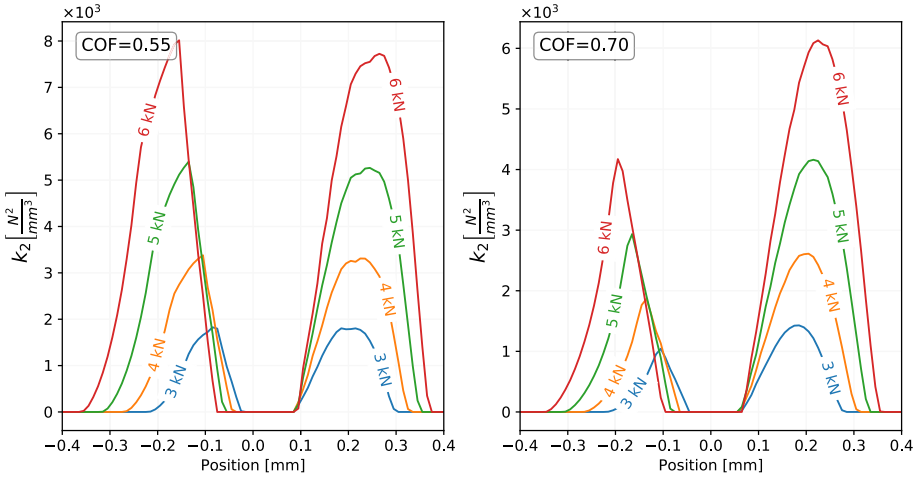

Fig. 6. Ruiz FFD parameter. The left and right peaks in each plot are the leading and trailing edges, respectively.

the maximum combination of shear stress amplitude and maximum normal stress over a stabilized cycle. Accordingly, maximising Eq. (4) yields the critical plane. Findley damage parameter is here denoted as F and may be expressed in a general three dimensional critical plane context as

$$F_{max} = \max_{\phi,\theta}\{F\} = \max_{\phi,\theta}\{\tau_a(\phi,\theta) + k\sigma_{n,max}(\phi,\theta)\} \quad (4)$$

where θ and ϕ are the first and second angular coordinates in a spherical coordinate system centered in the material point, see Fig. 7. k is a material parameter describing the material cracking sensitivity to normal stresses, and is determined based on experimental data. Higher values of k can be interpreted as increased sensitivity to *opening mode* effects on the shear cracks. k is therefore normally lower for shear dominated (ductile materials) than for brittle materials. Socie [35] propose to use 0.1–0.2 for ductile materials and Kallmeyer et al. [36] found 0.35 to give best correlation with uni-axial and bi-axial data for Ti-6Al-4V. A value of 0.35 was found to work well in this study. The damage function (F) in Eq. (4) can be thought of as the objective function to be maximised over

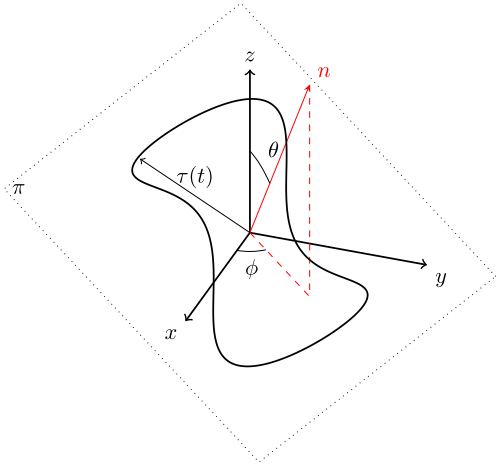

Fig. 7. Shear stress acting in the candidate plane π.

the space of possible material plane orientations and is visualized in Fig. 13. The damage F is plotted as a function of material plane orientation (θ,ϕ), but as the stress histories obtained from FEA in reality is a two-dimensional, critical plane needs only to be searched for over the angle ϕ. For the general 3D critical plane analysis using shear-based criteria, additional complexity is related to the problem of defining and computing *resolved shear stress amplitudes*. The shear stress history is a two-dimensional path in the candidate plane [37,38], as illustrated in Fig. 7. A very fine grid of angles (θ,ϕ) is obtained with angular increments of 1 degree. The resolved shear stress amplitudes used to compute the damage 13 are *computed with the maximum rectangular hull* (MRH) as demonstrated by Araújo et al. [38]. This algorithm calculates the shear amplitude by halving the largest diagonal of all rectangles enclosing the shear stress path in the candidate plane. Rectangles are computed by projecting the shear stress history on to a set of rotated coordinate axes in π. It has computational advantages over the more popular method of *minimum circumscribed circle* and handles non-proportionality better.

In terms of the number of cycles to initiate a crack, fatigue damage be expressed as [39]:

$$F_{max} = \tau_f^{'}(2N_f)^{b_0} \tag{5}$$

where $\tau_f^{'}$ is the shear stress fatigue strength, N_f is the number of cycles to initiate a crack and b_0, is the fatigue strength exponent. Material fatigue parameters were borrowed from [1]. The shear fatigue strength was calculated by

$$\tau_f^{'} = \frac{\sigma_f^{'}}{\sqrt{3}} \tag{6}$$

where $\sigma_f^{'}$ is the material uniaxial fatigue strength coefficient.

3.3. Theory of critical distances

It is well known that hot-spot fatigue evaluation over-estimate fatigue damage when steep stress gradients are present. This is indeed the case for fretting fatigue, where the subsurface stresses are high at the contact edges due to contact pressure and discontinuities in shear traction. A very steep stress gradient is clearly visible in Fig. 12, where fatigue damages are plotted for the specimen sub-surface. The peaks in shear stress at the slip edges are seen in Fig. 5. Using the *Theory of Critical Distances* (TCD), a material characteristic length (or depth) is used to evaluate a *process zone* in which the stresses are averaged by a certain criterion; using the *Point Method* the fatigue damage is calculated at the center of the process zone and for the *Volume Method* the stresses are averaged over the volume [1,40]. Here, the critical plane analyses are performed using both the Point Method and Volume Method. More specifically, the point method is implemented such that the fatigue life is evaluated at the critical point, defined as the material point at a distance $L/2$ from the hot-spot *along the hot-spot cracking direction*. Refer to Fig. 8. For the volume method, the fatigue damage is averaged over a ball (a circle in 2D case) of radius $L/2$ centered in the critical point.

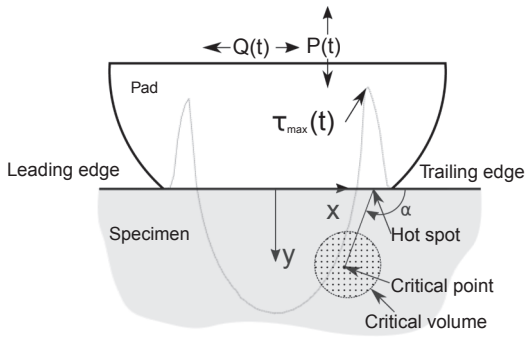

Fig. 8. Terminology for critical plane analysis using TCD. Note that the size and position of the critical volume is not necessarily in scale; in many cases it will reach the surface.

The numerical value of L is often related to the threshold stress intensity factor of the material from LEFM [41,42,29]

$$L = \frac{1}{\pi}\left(\frac{\Delta K_{th}}{\Delta\sigma_0}\right)^2 \tag{7}$$

where ΔK_{th} is the threshold stress intensity factor for crack fatigue growth and σ_0 is the plain fatigue limit [42]. Here, the value is calculated using material parameters from Dowling [43]. With $\Delta K_{th} = 5.5\ \text{MPa}\sqrt{\text{m}}$ and $\sigma_0 = 583\ \text{MPa}$ the critical distance L becomes approximately 28 μm. This value is in range of values used in [1] for the same material.

4. Results

Experimental results are shown in Table 3. A total of 15 tests, T1 through T15, were run until a stopping criterion was met or until run-out limit, which was set to two million cycles. The loads followed a sine-wave function with loading ratio $R = 0.1$ at 20 Hz. The loads in Table 3 are the peak (maximum) load for each specimen.

The two lowest loaded specimens were run-outs, see Fig. 14. All remaining specimens failed due to fretting fatigue, with cracks initiating from the near-center towards the trailing edge of contact and growing at an angle 50–60 degrees from the surface as seen in Fig. 9. Initiation angles seemed to be steeper for some samples as can be seen in Fig. 9b, however, comprehensive study of the crack initiation site proved to be difficult; cyclic contact pressure is still exerted on the fretted surface after the crack has been initiated, causing some small damage to the initiation sites. One can probably reduce this effect by defining more strict stopping criteria in the test configuration. Additionally, the latency introduced by peak-valley compensation caused some small damage to the initiation site.

Fractography using scanning electron microscope (SEM) confirmed that in general, cracks formed under the contact inside the slip region near the theoretical point of initial contact (see Fig. 10b). As can be seen in Fig. 10a, the EDM wired surface is very irregular and rough, with melted drops and potential surface defects. The melted drops are vulnerable to plastic flow as the pad comes into contact with the specimen and are probably subjected to plowing during early sliding, as can be observed as furrows in Fig. 10a around the edge of contact. Since the contact is cylindrical in profile, particle ejection is mostly unhindered, promoting wear. Debris particles caused by wear are seen on the fretted surface and at the edge of contact.

A subset of specimens were equipped with strain gauges on each side, as illustrated in Fig. 2. An example of the monitored strains are post-processed and plotted in Fig. 11 for T12. Here, peaks and troughs are extracted from the continuous signal and shown as separated lines for each side. Notice how the strain range is slightly higher on the left side of the specimen even though the opposite side is the one to experience the fretting fatigue crack. Peak strains on the right side is slowly decreasing from early on, even though the left strain is fairly constant until around $8.5{\cdot}10^5$. Then, as the crack grows, strains quickly change. Peaks and troughs are also shown for the overall displacement of specimen during its lifetime. The transient response during the first few cycles after loading is first probably dominated by fluid film effects in the U-joint followed by some small contact plastic flow. The contact eventually reaches elastic shakedown after which the response is relatively stable, until sudden crack growth and failure. Displacements are slowly increasing during the first few 100 k cycles until it stabilizes. This can be due to increased wear and easy particle ejection during the early fretting life, when the unworn Hertzian profile cause high contact stresses and wear. By evaluating the increase in displacements, the onset of crack

Table 3
Experimental test results. Samples marked with * were run-outs.

Test	T1	T2*	T3	T4	T5*	T6	T7	T8
Load [kN]	5.00	3.00	4.00	4.50	3.50	6.00	3.75	4.25
Cycles	377972	2e6	1869836	952207	2e6	313831	1016966	1648296
Test	T9	T10	T11	T12	T13	T14	T15	
Load [kN]	6.50	5.00	5.50	4.00	4.80	4.20	5.20	
Cycles	284403	624729	590233	1025609	722932	1293027	724374	

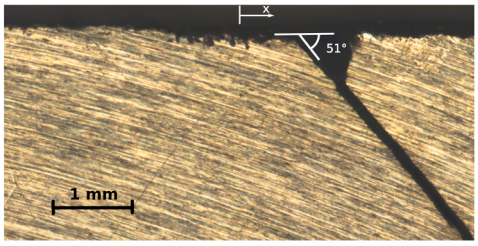

(a) Cracking direction for sample T6.

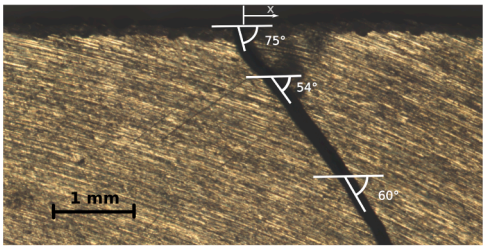

(b) Cracking direction for sample T9.

Fig. 9. Two typical cracking angles. Contact center and positive sliding direction is annotated by the arrow. The visible textures on the specimen sides are due to being machined flat.

failure is demonstrated by dotted lines and found in general to be 90–95% of overall specimen life.

Separating fretting fatigue crack initiation life from the overall fatigue life is in general an elusive problem. The definition of defect size for which the transition from initiation phase to growth phase is not unequivocally defined. Additionally, the relative importance of one phase over the other is in general not known. As noted by Navarro et al. [44], this transition may depend upon the fatigue criterion used, loading condition, material, geometry, etc. and cannot be known *a priori*. If the crack growth phase was to be significant, a modelling technique from *Linear-Elastic Fracture Mechanics* (LEFM) could be used to subtract the long crack growth regime. Here however, the fretting crack nucleation/initiation life is assumed to be 90% of overall specimen fatigue life. This is obviously a generalisation, but is perhaps somewhat justified by the recorded "fretting maps" (see Fig. 11). Also, previous researchers have reported initiation life in fretting fatigue of 85–95% [45–47].

4.1. Numerical post-processing

From the FE analysis, stresses and strains are extracted for a subset of 20,000 material points representing the specimen subsurface. By post-processing the FE results using the Findley critical plane parameter, the entire load history is conveniently transformed to a vector field representing fatigue damage. The length of each vector represents the fatigue damage in the material point and the angle represents the cracking direction. Fig. 12 demonstrates the subsurface fatigue damage for test cases T2 and T6 for two different values of COF. The hot-spot is marked with its cracking direction vector by an arrow. The figure clearly shows the steep gradients in the surface region, and highlights the edges of contact as being the critical areas. Generally, trailing edge ($x = 0.45$) of contact is found to be the hot-spot, as expected. The shapes of the critical areas at contact edges are elongated due to the slip interface changing throughout the loading cycle, thus "smearing" fatigue damage.

Findley fatigue damage parameter can also be plotted for single material points as a function of 3D material plane orientation (θ, ϕ), see Fig. 13. Here, the damage is calculated for a grid of 180x180 different material plane orientations for the hot-spot and critical point for load case T2. Due to the FE assumption of plane strain in the contact area, one only need to search through one dimension of angles. Note the symmetry of the damage parameter around $\theta = 90°$.

Negative values of the Findley parameter are due to small values for the resolved shear amplitude and with negative (compressive) normal stresses acting on the plane. Recall Eq. (4). Numerical simulations show that the Findley parameter is very sensitive to coefficient of friction for this geometry. Larger friction force gives higher shear stresses near the surface.

The experimental results is plotted with a set of numerical predictions in Fig. 14. The effect of increasing COF is unsurprising. Life predictions made without TCD are obviously over-conservative, however by using a critical distance found based on El Haddad [41],

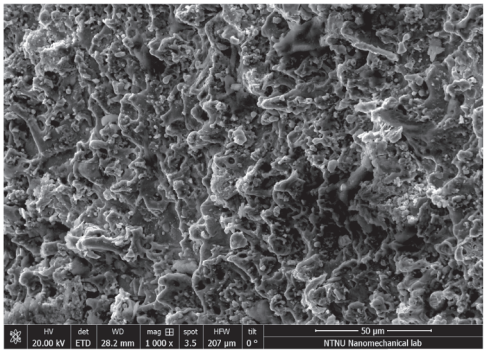

(a) EDM wired surface.

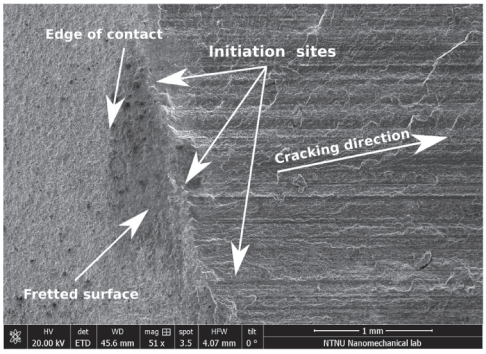

(b) Fretted surface meets crack surface

Fig. 10. Scanning electron microscope image of fractured surface.

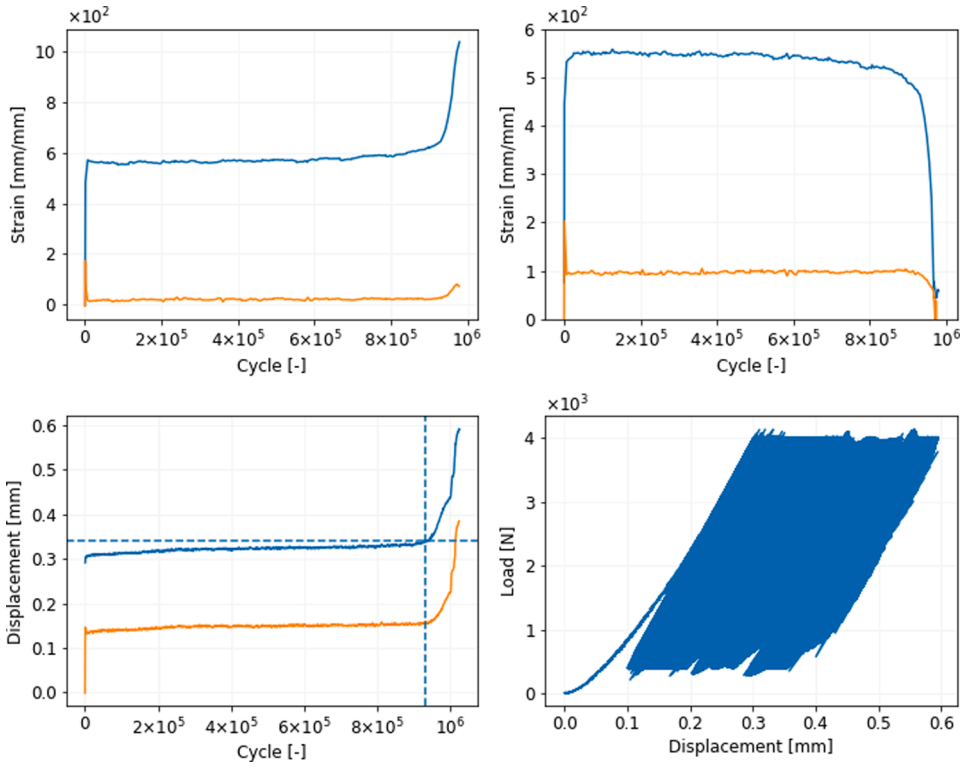

Fig. 11. *In-situ* monitoring specimen behaviour (test T12).

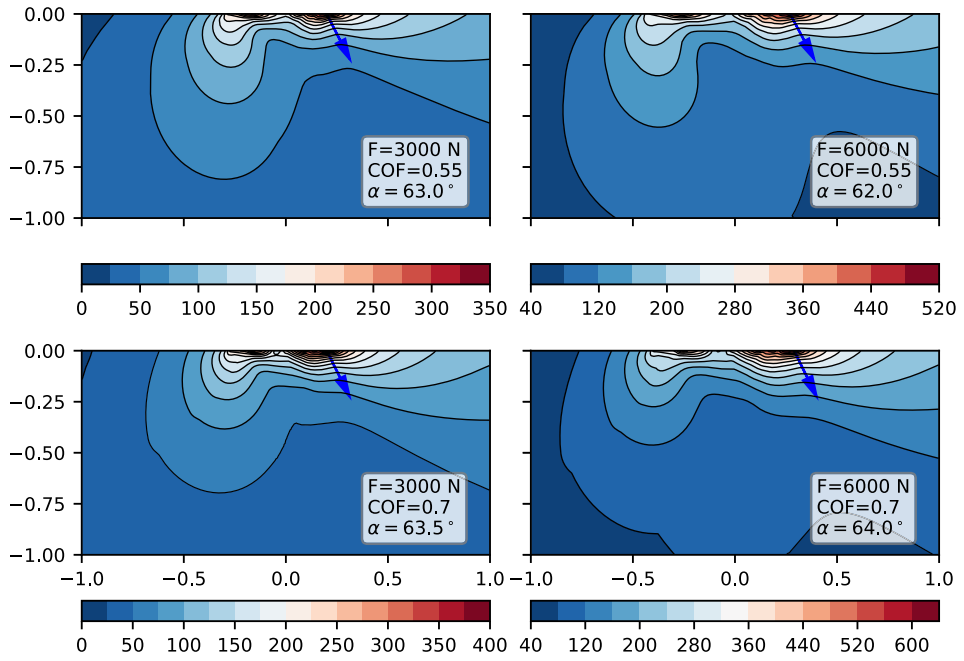

Fig. 12. Subsurface Findley damage parameter with hot-spot cracking direction indicated by arrow.

predictions are significantly improved. It is clear, however, that the slopes seen in the experimental results are different from the numerical predictions and so the inaccuracy increase as the loads are reduced. With respect to wear, this is slightly unexpected as wear often is thought to wipe out potential initiation sites, resulting in longer lives. The abrupt change in life prediction using the point method shows how evaluation of fatigue life at a single point is somewhat sensitive to spatial perturbations.

5. Discussion

The demonstrated test-rig is inspired by the classical dovetail fixture designs and its many descendants; however, it has a number of small additions which makes it capable of testing and comparing a wide range of fretting fatigue conditions. The width of the gripping mechanism permits specimens of different sizes to be tested. Additionally, the possibility of enclosing the lower gripping flange enable tests to be run in submerged conditions. In a multi-axial test machine with combined

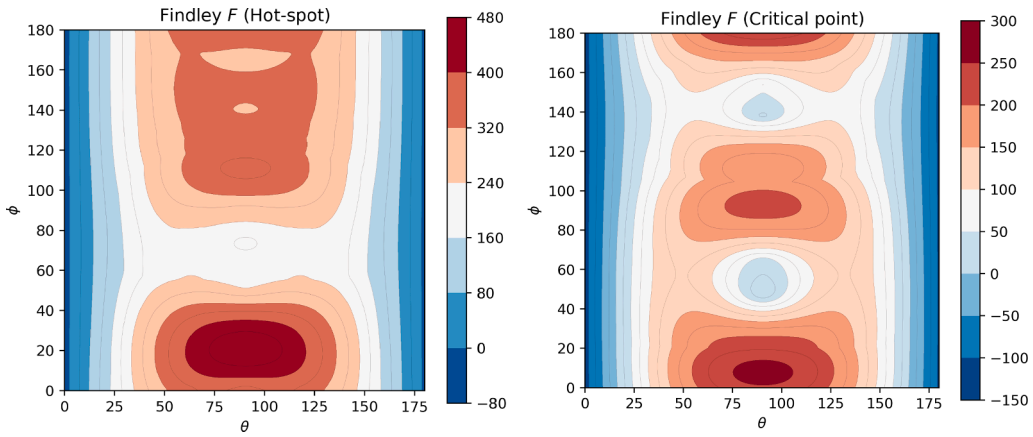

Fig. 13. Comparing candidate plane fatigue damage for the hot-spot (left) and at critical distance (right). Notice how the symmetries reveal the two-dimensional nature of the FE model.

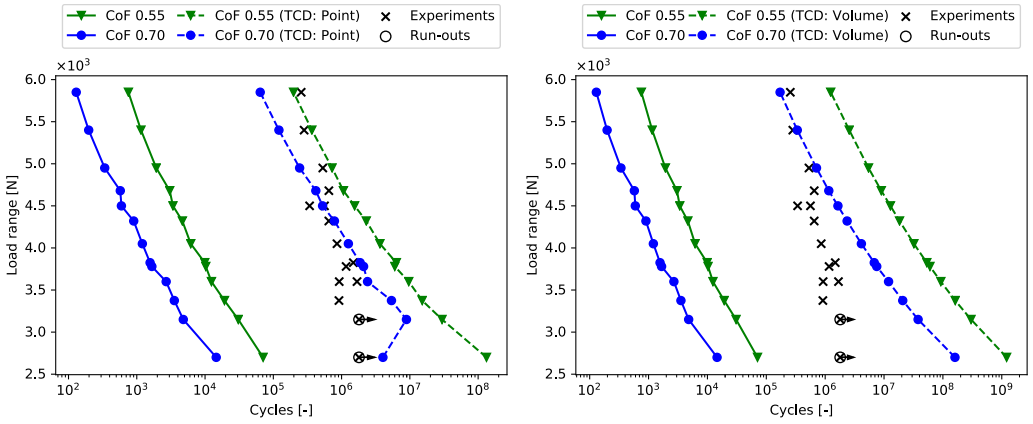

(a) Load-life using Point method. (b) Load-life using Volume method.

Fig. 14. Experimental results with numerical predictions using Findley criterion and TCD. Notice the "kink" in predicted life using the point method. This shows the potential instability when evaluating fatigue damage at a single point for very steep stress gradients.

tension-torsion actuators, additional excitation can be exerted on the specimens. In this study however, only single specimens were tested in dry conditions in room temperature.

A total of 15 EDM wired Ti-6Al-4V specimens were tested using the new rig resulting in fatigue failure initiated from the contact. To accompany the experimental data, numerical simulations were performed using finite element methods. Linear-elastic stress results were post-processed using Ruiz parameters and critical plane using the Findley criterion. In general, Ruiz provided insights into the critical areas, but failed to give meaningful life-predictions. The Findley criterion proved to be reasonable accurate in predicting crack angle and life when combined with the Theory of Critical Distances and length parameter based on LEFM.

Specimens were monitored during testing using strain gauges collecting large amounts of data. Post-processing the running data collection can potentially give valuable insights into fretting fatigue using appropriate data analysis.

The numerical model used to correlate life predictions with experimental results is evidently simplified. Like in many engineering applications, the analyses relied on bulk material properties, technical standards and assumptions made for contact friction. One potential next development step for the numerical model is to include wear analyses, but as noted by [29], the added computational cost is not always justified. Specimens in this test program were mostly in mixed regime between partial slip and gross slip. It is hypothesised that the inclusion of wear in the numerical model presented here will improve accuracy. Plasticity effects are not accounted for either, but was only observed in small, localized amounts related to the rough surfaces from the EDM wiring process. Work is initiated to add routines to handle plasticity and wear to the numerical model.

The new test rig demonstrated in this works has thus far only been used in its most simple configuration: Dry contact and uniaxially loaded specimens with cylindrical (Hertzian) contact pads. A planned advancement experimentally is to apply additional excitations to the specimens using the torsion actuators. Also of interest is to enclose the dovetail chamber and test specimens in submerged conditions. Changing the contact geometry to complete or rounded-flat will increase the resemblance with actual dovetail joints, increase contact stick and change the surface stress concentrations.

6. Conclusion

A combined experimental and numerical study has been conducted, using a new fretting fatigue test rig based on the classical dovetail joint. The main aim of this project is to initiate a new capacity for performing fretting fatigue experiments and associated numerical analysis. The project provides groundwork for future fretting fatigue test programs and parameter studies. The test setup has been demonstrated on a set of EDM-wired specimens in an engineering context, using bulk material properties and assumptions made for the coefficient of friction. The test

rig is concluded to be appropriate for detailed studies of fretting fatigue where material properties are of interest. This relies on explicit measurements of the system coefficient of friction and carefully controlled material properties and contact surfaces.

Declaration of Competing Interest

The authors declare that they have no known competing financial interests or personal relationships that could have appeared to influence the work reported in this paper.

Acknowledgements

xxx

References

[1] Araújo JA, Nowell D. The effect of rapidly varying contact stress fields on fretting fatigue. Int J Fatigue 2002;24(7):763–75. https://doi.org/10.1016/S0142-1123(01)00191-8. ISSN: 0142-1123. URL: http://www.sciencedirect.com/science/article/pii/S0142112301001918.

[2] Nowell D, Dini D, Hills DA. Recent developments in the understanding of fretting fatigue. Eng Fract Mech 2006;73(2):207–22. https://doi.org/10.1016/j.engfracmech. 2005.01.013. Advanced Fracture Mechanincs for Life Safety Assessments. ISSN: 0013-7944. URL: http://www.sciencedirect.com/science/article/pii/S0013794405001803.

[3] Lindley TC, Nix KJ. Fretting fatigue in the power generation industry: experiments, analysis, and integrity assessment. In: Standardization of fretting fatigue test methods and equipment. ASTM International; 1992. p. 153–17. doi: 10.1520/stp25828s.

[4] Ruiz C, Boddington PHB, Chen KC. An investigation of fatigue and fretting in a dovetail joint. Exp Mech 1984;24(3):208–17. https://doi.org/10.1007/BF02323167. ISSN: 1741-2765.

[5] Ciavarella M, Demelio G. A review of analytical aspects of fretting fatigue, with extension to damage parameters, and application to dovetail joints. Int J Solids Struct 2001;38(10):1791–811. https://doi.org/10.1016/S0020-7683(00)00136-0. ISSN: 0020-7683. URL: http://www.sciencedirect.com/science/article/pii/S0020768300001360.

[6] Conner BP, Nicholas T. Using a dovetail fixture to study fretting fatigue and fretting palliatives. J Eng Mater Technol 2006;128(2):133. https://doi.org/10.1115/1.2172272.

[7] Golden Patrick J. Development of a dovetail fretting fatigue fixture for turbine engine materials. Int J Fatigue 2009;31(4):620–8. https://doi.org/10.1016/j.ijfatigue.2008.03.017.

[8] Chen J-J, et al. Experimental and numerical investigation on crack initiation of fretting fatigue of dovetail. Fatigue Fract Eng Mater Struct 2018;41(6):1426–36. https://doi.org/10.1111/ffe.12787.

[9] Rajasekaran R, Nowell D. Fretting fatigue in dovetail blade roots: Experiment and analysis. Tribol Int 2006;39(10):1277–85. https://doi.org/10.1016/j.triboint.2006.02.044.

[10] Hills DA, Nowell D. What features are needed in a fretting fatigue test? In: Tribology International 42.9. Special Issue: Fifth International Symposium on Fretting Fatigue; 2009. p. 1316–23. https://doi.org/10.1016/j.triboint.2009.04.023. ISSN: 0301-679X. URL: http://www.sciencedirect.com/science/article/pii/S0301679X09000905.

[11] Hills DA, Nowell D. Mechanics of fretting fatigue-Oxford's contribution. Tribol Int 2014;76:1–5. https://doi.org/10.1016/j.triboint.2013.09.015.

[12] Kartal ME, et al. Determination of the frictional properties of titanium and nickel alloys using the digital image correlation method. Exp Mech 2010;51(3):359–71. https://doi.org/10.1007/sll340-010-9366-y.

[13] De Pauw J, et al. On the use of digital image correlation for slip measurement during coupon scale fretting fatigue experiments. Int J Solids Struct 2014;51(18):3058–66. https://doi.org/10.1016/j.ij solstr.2014.05.002.

[14] Juoksukangas J, Lehtovaara A, Mantyla A. Applying the digital image correlation method to fretting contact for slip measurement. Proc Inst Mech Eng Part J: J Eng Tribol 2016;231(4):509–19. https://doi.org/10.1177/1350650115601695.

[15] Kyvia Pereira et al. On the convergence of stresses in fretting fatigue. In: Materials 9.8; July 2016. p. 639. DOI: 10.3390/ma9080639.

[16] Fouvry S, Duo P, Perruchaut Ph. A quantitative approach of Ti-6A1-4V fretting damage: friction, wear and crack nucleation. Wear 2004;257(9–10):916–29. https://doi.org/10.1016/j.wear.2004.05.011.

[17] Suh Nam P, Sin H-C. The genesis of friction. In: Wear 69.1; June 1981. p. 91–114. DOI: 10.1016/0043-1648(81)90315-x.

[18] Yue Tongyan, Wahab Magd Abdel. Finite element analysis of fretting wear under variable coefficient of friction and different contact regimes. Tribol Int 2017;107:274–82. https://doi.org/10.1016/j.triboint.2016.11.044.

[19] Sunde Steffen Loen, Berto Filippo, Haugen Bjorn. Efficient implementation of critical plane for 3D stress histories using triangular elements. Int J Fatigue 2020;134:105448. https://doi.org/10.1016/j.ijfatigue.2019.10544.

[20] Mindlin RD. Compliance of Elastic Bodies in Contact. J Appl Mech ASME 1949;16:259–68.

[21] Ciavarella M. Transition from stick to slip in Hertzian contact with Griffith friction: The Cattaneo-Mindlin problem revisited. J Mech Phys Solids 2015;84:313–24. https://doi.org/10.1016/j.jmps.2015.08.002.

[22] Lykins Christopher D, Mall Shankar, Jain Vinod. An evaluation of parameters for predicting fretting fatigue crack initiation. Int J Fatigue 2000;22(8):703–16. https://doi.org/10.1016/S0142-1123(00)00036-0. ISSN: 0142-1123. URL: http://www.sciencedirect.com/science/article/pii/S0142112300000360.

[23] Ziaei M. Analytical study of noncircular profile families andnumerical optimization of standardised polygon profiles for shaft-hub connections. Professorial Dissertation; 2002.

[24] Ding J, Leen SB, McColl IR. The effect of slip regime on fretting wear-induced stress evolution. Int J Fatigue 2004;26(5):521–31. https://doi.org/10.1016/j.ijfatigue.2003.09.001. ISSN: 0142-1123. URL: http://www.sciencedirect.com/science/article/pii/S0142112303002032.

[25] Vidner J, Leidich E. Enhanced Ruiz criterion for the evaluation of crack initiation in contact subjected to fretting fatigue. Int J Fatigue 2007;29(9-11):2040–9. https://doi.org/10.1016/j.ij fatigue.2007.02.010.

[26] Sunde SL, Berto F, Haugen B. Predicting fretting fatigue in engineering design. Int J Fatigue 2018;117:314–26. https://doi.org/10.1016/j.ijf atigue.2018.08.028.

[27] Strozzi A, et al. A repertoire of failures in connecting rods for internal combustion engines, and indications on traditional and advanced design methods. Eng Fail Anal 2016;60:20–39. https://doi.org/10.1016/j.engf ailanal. 2015.11.034.

[28] Ding J, et al. Simple parameters to predict effect of surface damage on fretting fatigue. Int J Fatigue 2011;33(3):332–42. https://doi.org/10.1016/j.ijf atigue. 2010. 09. 008.

[29] Araujo JA, et al. Life prediction in multiaxial high cycle fretting fatigue. Int J Fatigue 2020;134:105504. https://doi.org/10.1016/j.ij fatigue.2020.105504.

[30] Nowell D, Hills DA. Crack initiation criteria in fretting fatigue. Wear 1990;136(2):329–43. https://doi.org/10.1016/0043-1648(90) 90155-4.

[31] Fouvry Siegfried, Kapsa Philippe, Vincent Leo. Quantification of fretting damage. Wear 1996;200(1–2):186–205. https://doi.org/10.1016/s0043-1648(96)07306-l.

[32] Vantadori Sabrina, et al. Early fretting crack orientation by using the critical plane approach. Int J Fatigue 2018;114:282–8. https://doi.org/10.1016/j.ijfatigue.2018.04.015.

[33] Sum WS, Williams E, Leen S. Finite element, critical-plane, fatigue life prediction of simple and complex contact configurations. Int J Fatigue 2005;27(4):403–16. https://doi.org/10.1016/j.ijfatigue.2004.08.001.

[34] Nicholas Findley W. A theory for the effect of mean stress on fatigue of metals under combined torsion and axial load or bending. Engineering Materials Research Laboratory, Division of Engineering, Brown University; 1958.

[35] Socie Darell F, Marquis Gary B. Multiaxial fatigue. SAE International: Marquis. Multiaxial fatigue; 2000. ISBN: 9780768004533.

[36] Kallmeyer Alan R, Krgo Ahmo, Kurath Peter. Evaluation of multiaxial fatigue life prediction methodologies for Ti-6A1-4V. J Eng Mater Technol 2002;124(2):229–37. https://doi.org/10.1115/1.1446075.

[37] Papadopoulos IV. Critical plane approaches in high-cycle fatigue: on the definition of the amplitude and mean value of the shear stress acting on the critical plane. Fatigue Fract Eng Mater Struct 1998;21(3):269–85. https://doi.org/10.1046/j.1460-2695.1998.00459.x.

[38] Araujo JA, et al. On the characterization of the critical plane with a simple and fast alternative measure of the shear stress amplitude in multiaxial fatigue. Int J Fatigue 2011;33(8):1092–100. https://doi.org/10.1016/j.ijfatigue.2011.01.002. Multiaxial Fatigue Models, . ISSN: 0142-1123. URL: http://www.sciencedirect.com/science/article/pii/S0142112311000041.

[39] Park J. Evaluation of an energy-based approach and a critical plane approach for predicting constant amplitude multiaxial fatigue life. Int J Fatigue 2000;22(1):23–39. https://doi.org/10.1016/s0142-1123(99)00111-5.

[40] Susmel Luca, Taylor David. Non-propagating cracks and high-cycle fatigue failures in sharply notched specimens under in-phase Mode I and II loading. Eng Fail Anal 2007;14(5):861–76. https://doi.org/10.1016/j.engfailanal.2006.11.038.

[41] El Haddad MH, Smith KN, Topper TH. Fatigue crack propagation of short cracks. J Eng Mater Technol 1979;101(1):42. https://doi.org/10.1115/1.3443647.

[42] Taylor D. Geometrical effects in fatigue: a unifying theoretical model. Int J Fatigue 1999;21(5):413–20. https://doi.org/10.1016/s0142-1123(99)00007-9.

[43] Dowling Norman E. Mechanical behaviour of materials. Pearson Education Limited; 2013.

[44] Navarro C, Mufioz S, Dominguez J. On the use of multiaxial fatigue criteria for fretting fatigue life assessment. Int J Fatigue 2008;30(1):32–44. https://doi.org/10.1016/j.ijfatigue.2007.02.018.

[45] Szolwinski Matthew P, Farris Thomas N. Mechanics of fretting fatigue crack formation. Wear 1996;198(1–2):93–107. https://doi.org/10.1016/0043-1648(96)06937-2.

[46] Lykins C. Combined experimental-numerical investigation of fretting fatigue crack initiation. Int J Fatigue 2001;23(8):703–11. https://doi.org/10.1016/s0142-1123(01)00029-9.

[47] Shi Liang, et al. An investigation of fretting fatigue in a circular arc dovetail assembly. Int J Fatigue 2016;82:226–37. https://doi.org/10.1016/j.ijfatigue.2015.07.025.